Alkali Metal Doping of MgO: Mechanisms of Formation of Paramagnetic Surface Centers

Silvia Brazzelli, Cristiana Di Valentin, and Gianfranco Pacchioni*

Dipartimento di Scienza dei Materiali, Università di Milano-Bicocca, Istituto Nazionale per la Fisica della Materia, Via R. Cozzi, 53 - 20125, Milano, Italy

Elio Giamello and Mario Chiesa

Dipartimento di Chimica IFM, Università di Torino, and Istituto Nazionale per la Fisica della Materia, via P. Giuria 5, I-10125 Torino, Italy

Received: January 17, 2003; In Final Form: April 1, 2003

The adsorption of alkali-metal atoms (M = Li, Na, and K) on the surface of MgO has been studied by means of embedded-cluster DFT calculations. Alkali-metal atoms bind preferentially to the oxide anions with energies of the order of 1 eV. On these sites the *n*s valence electron remains localized on the alkali atom, but the substantial polarization (*n*s−*n*p mixing) leads to major changes in the isotropic hyperfine coupling constants. In the presence of specific defect sites, like a bare oxygen vacancy, F_S^{2+} center, a net charge transfer occurs, with formation of F_S^{+} color centers. At higher coverages, once the F_S^{2+} centers have been saturated, a different process takes place. At specific neutral morphological defects, like a cationic reverse corner, the alkali atom valence electron is transferred to the surface with formation of $M^+(e^-)_{trapped}$ pairs. The computed properties of the unprecedented $M^+(e^-)_{trapped}$ pairs (hyperfine constants and optical transitions) are consistent with the experimental measures and show that the trapped electron and the adsorbed alkali-metal cation are separated by short distances.

1. Introduction

The study of the deposition of metal atoms, clusters, and films on oxide surfaces is a subject attracting a growing interest.[1,2] One of the most studied systems in this context is MgO, a prototype of ionic oxides with NaCl-like cubic structure, and a special case of metal deposition is that of alkali metals which can give rise to various situations, from creation of color centers, to the formation of metal overlayers.[3] It becomes increasingly clear that point defects have a crucial role in the nucleation and growth of the metal on the surface. Among the several possible MgO defects,[4,5] anion and cation vacancies (F_S and V_S centers, respectively, with S = surface) are often considered to be involved in the interaction of the deposited metal with the surface.[6−23] F_S and V_S centers exists in various charge states. The removal of O, O^-, or O^{2-} results in the formation of F, F^+, and F^{2+} centers, respectively; in a similar way, the removal of Mg, Mg^+, or Mg^{2+} results in V, V^-, and V^{2-} centers. F_S centers are strong basic sites which donate charge and modify the chemical activity of metal atoms, clusters, or molecules;[24,25] on the other extreme, F_S^{2+} centers are strong acid sites which are able to ionize metal deposits and individual atoms. V_S centers have attracted considerably less interest.[4]

In this work the deposition of alkali atoms on the MgO surface has been modeled by DFT cluster model calculations. At low doses of deposited metal, mainly atoms are present on the surface, and only at higher coverages small alkali aggregates begin to form. We have considered the adsorption of isolated Li, Na, and K atoms on cation and anion sites of the surface and the formation of ionized species, like Na^+ and trapped electrons. We have analyzed the possible precursor sites of the trapped electrons and the mechanisms which lead to the formation of paramagnetic centers at the surface of MgO as a function of the coverage. Thus, adsorption at regular and defect sites has been considered. In particular, alkali-metal atoms have been adsorbed at F centers or morphological irregularities on the surface. The model of a F center consists of five Mg cations in a square-pyramidal arrangement.[26,27] For almost 30 years this model (Tench's model) has been used to interpret experimental data or to construct local models of paramagnetic centers at the surface of MgO.[28−41] In this paper we show, for the first time, that beside the classical ionization of the alkali metals induced by strongly electron deficient centers such as the doubly charged oxygen vacancies, F^{2+}, another mechanism contributing to the formation of paramagnetic color centers is connected with the formation of $(M^+)(e^-)_{trapped}$ pairs where the electron is trapped at some specific neutral MgO surface sites.

The paper is organized as follows. In section 2 we describe the computational method used. The results are divided into three parts: adsorption of neutral atoms on cation and anion sites of the surface (section 3.1), adsorption of alkali-metal cations (section 3.2), and ionization of alkali metals (section 3.3). In Section 4 we discuss the spin distribution and we compare the computational results with the experimental ones. Section 5 summarizes our conclusions.

2. Details of Calculations

Density functional theory (DFT) quantum-mechanical calculations were carried out by using the gradient-corrected Becke's three parameters hybrid exchange functional[42] in combination with the correlation functional of Lee, Yang, and Parr[43] (B3LYP).

To calculate the properties of Li, Na, and K atoms deposited on the MgO surface, we employed two different embedded

* Corresponding author. E-mail: gianfranco.pacchioni@unimib.it.

10.1021/jp0341321 CCC: $25.00
Published on Web 07/16/2003

cluster approaches. In the first one the MgO (100) surface is represented by finite MgO clusters embedded in ±2 point charges (PC). The large array of PC's reproduces the Madelung potential at the adsorption site.[44] To avoid the artificial polarization of the O^{2-} anions at the cluster border induced by the PC's,[45−48] we have replaced the positive PC's at the interface by effective core potentials (ECPs)[49] which provide a representation of the finite size of the cation. The interface Mg cations treated in this way are denoted in the following as Mg*. No basis functions are associated to these atoms. This approach has been used in the past in a number of cases and compared carefully to periodic approaches and more elaborate embedding schemes based on Green functions.[50] The results are virtually the same, showing that the electrostatic potential in the cluster region provided by the set of point charges correctly reproduces that of the extended surface. The PC-embedded cluster does not account for long-range polarization and geometrical relaxation effects, which become particularly important for charged systems. Various MgO adsorption sites have been considered: regular (100) terraces, low coordinated ions (i.e., edge or step sites), and the reverse corners, the sites originating from the intersection of two steps. Notice that there are two types of reverse corners: one centered on a Mg cation and characterized by two O_{4c} and one O_{5c} anions forming a triangular adsorption site and one centered on a O anion and characterized by two Mg_{4c} and one Mg_{5c} cations. In the following the two sites are referred to as anionic reverse corner, MgO_{ARC}, and cationic reverse corner, MgO_{CRC}, respectively. In PC-embedded clusters the central Mg and O atoms near the adsorption site have been described with a 6-31+G* basis set, while the remaining atoms have been treated with the 6-31G basis. The calculations have been performed by using the Gaussian-98 program package.[51]

The calculations for M and M^+ cations adsorbed on MgO have been done starting from the neutral M/MgO cluster complex and then removing one electron from the system. This introduces important electronic relaxation effects due to the presence of a positive charge. Long-range polarization effects have been taken into account in a second approach. In this case the MgO crystal has been represented by a large cluster, divided into regions I and II. Region I includes a quantum-mechanically treated cluster (QM cluster) surrounded by interface ions and classical shell model ions.[76,52] The remaining part of the cluster, region II, is represented by PC's. All the classical ions interact among themselves via interatomic potentials. The interface atoms interact quantum mechanically with the QM cluster and classically with atoms in regions I and II. The interaction between the QM atoms and classical atoms in regions I and II is also included and is described by short-range classical potentials. All centers in region I are allowed to relax simultaneously during the geometry optimization. PC's in region II remain fixed and provide an accurate electrostatic potential (EP) within region I. Also here an interface between QM cluster and classical ions is needed in order to prevent an artificial spreading of electronic states outside the QM cluster and is based on the representation of the Mg^{2+} ions by ECP's[49] as described above. This hybrid scheme is implemented in the GUESS code,[36] which provides the shell model representation for the classically treated part of the system and an interface with the Gaussian98 package for ab initio calculations[51] of the QM cluster. The GUESS code allows us to calculate forces acting on all centers in region I, both QM and classical (cores and shells), and simultaneously optimize their positions by using the Broyden-Fletcher-Goldfarb-Shanno technique[53] for the energy minimization. We denote these clusters as shell-model embedded clusters (SM-embedded).

TABLE 1: Atomic Properties of Li, Na, and K Atoms Obtained at the B3LYP Level with Various Basis Sets

atom	basis set	IP,[a] eV	α^b	a_{iso},[c] G
Li	3-21G	5.59	20.5	113.3
	3-21G*	5.59	20.5	113.3
	3-21+G*	5.59	21.1	114.1
	6-31G	5.62	17.7	133.2
	6-31G*	5.62	17.8	133.2
	6-31+G*	5.62	20.4	129.4
	6-311+G*	5.62	20.8	155.5
	exptl	5.39[b]	24.3[b]	143.3[c]
Na	3-21G	5.36	20.6	189.3
	3-21G*	5.36	21.0	189.3
	3-21+G*	5.36	22.3	189.1
	6-31G	5.41	20.0	224.9
	6-31G*	5.41	20.1	224.9
	6-31+G*	5.41	21.5	224.7
	6-311+G*	5.42	21.4	334.7
	exptl	5.14[d]	23.6[d]	316.1[e]
K	3-21G	4.45	36.5	43.0
	3-21G*	4.45	37.1	43.0
	6-31G	4.48	35.5	54.5
	6-31G*	4.48	35.4	54.5
	6-31+G*	4.48	43.8	54.5
	6-311+G*	4.50	41.5	83.9
	exptl	4.34[b]	43.4[b]	82.5[c]

[a] IP = ionization potential. [b] $\alpha_\mu' = \alpha_\mu/4\pi\epsilon_o[10^{-24}\ cm^3]$ = polarizability. [c] a_{iso} = isotropic hyperfine coupling constant. [d] Ref erence 58. [e] Reference 59.

The standard 6-31G basis set[54,55] for Mg and O atoms was used in the calculations in order to allow a direct comparison of the results for alkali atoms with those recently reported on the dissociation of the H_2 molecule on the same surface.[56] Thus, slightly different basis sets have been used for PC-embedded and SM-embedded clusters. In some cases, also the composition of the PC- and SM-embedded clusters differs slightly.

Various basis sets have been used on the alkali metals with the objective to reproduce accurately three important atomic properties, Table 1: the ionization potential (IP), the polarizability, α,[57] and the isotropic part of the hyperfine coupling constant, a_{iso} (see below). The IP and the polarizability are essential to obtain a good description of the charge transfer or covalent bonding of the metal atom to the surface; a good reproduction of the atomic hyperfine interaction is needed for comparison with experimental results.[58,59] It turns out that the 6-311+G* basis set provides an overall agreement with experiment for all three quantities of interest and for all atoms, Li, Na, and K, Table 1, and has thus been used in all the calculations. The interaction energies have been corrected by the basis set superposition error (BSSE) using the counter-poise correction.[60]

The excitation energies of the trapped electron have been computed by using the time-dependent density functional approach (TD-DFT). For molecular systems, TD-DFT is known to provide a good accuracy,[61−63] while relatively few examples of applications to optical transitions of defects in solids have been reported.[64]

The hyperfine interaction, $A = a_{iso} + \mathbf{B}$,[65] of the electron spin with the nuclear spin of the ^{25}Mg and alkali-metal nuclides has been determined and compared with the experimental values. The isotropic part, a_{iso}, of each coupling constant is related to the spin density at the nucleus (the Fermi contact term):

$$a_{iso} = (2\mu_o/3)g_N\beta_N g_e\mu_B\langle\rho^s\rangle \qquad (1)$$

where μ_o is the permeability of free space, g_N is nuclear g-factor, g_e is the electronic g-factor for the site under consideration, β_N

TABLE 2: Adsorption Properties of a Neutral Na Atom on Various Cations Sites of the MgO Surface as Modeled by PC-Embedded Clusters[a]

	terrace	edge	corner
d(Na−Mg), Å	3.32	3.48	3.46
D_e, eV	0.14	0.09	0.25
D_e(BSSE), eV	0.08	0.05	0.17
ω_e,[b] cm^{-1}	73	78	95
q(Na)	−0.17	0.08	0.23
spin(Na)	1.10	0.89	0.72
a_{iso}(Na), G	301.8	313.7	310.7
a_{iso}(Mg), G	−0.1	−0.8	−5.6

[a] d(Na−Mg) = shortest Na−Mg distance; D_e = dissociation energy; D_e(BSSE) = dissociation energy corrected by the BSSE; ω_e = Na−MgO vibrational frequency; q(Na) = net charge on Na from Mulliken population; spin(Na) = spin population on Na; a_{iso} = isotropic hyperfine coupling constant. [b] Determined by polynomial fitting of the potential energy curve computed by single-point calculations.

and μ_B are the nuclear and Bohr magnetons, and $\langle\rho^s\rangle$ is the expectation value at the nucleus of the spin-density operator. In one-electron systems, $\langle\rho^s\rangle = |\Psi^s(0)|^2$. The anisotropic traceless tensor B results from the dipolar interaction:

$$B_{ij} = (\mu_o/4\pi)g_N\beta_N g_e\mu_B\int(3x_ix_j/r^5 - \delta_{ij}/r^3)|\Psi(r)|^2\,dV \quad (2)$$

3. Results and Discussion

3.1. Adsorption of Neutral Atoms on MgO. The first question to address is where the isolated alkali-metal atoms impinging on the surface from the metal vapor will bind preferentially. On the regular terrace sites of the MgO(100) surface the two possibilities are represented by the five-coordinated cations, Mg_{5c}^{2+}, or anions, O_{5c}^{2-}. Bridge-bonded situations are also possible but previous studies on the adsorption of transition-metal atoms have shown that these are saddle points in the diffusion of the atoms on the surface.[66] Transition- and alkali-metal atoms prefer to adsorb on the oxide anions;[67,68] a previous study on the adsorption of Rb on MgO performed at the Hartree−Fock level predicted no binding on the O sites and a weak binding at the cation sites,[69] but this result is affected by the lack of correlation effects. Of course, the bonding can be quite different at low-coordinated sites. Thus, the study has been extended also to some of these sites using Na as a representative atom of the group.

3.1.1. Interaction of the Na Atom with Mg^{2+} Cations. A neutral Na atom has been placed above a Mg^{2+} cation at a terrace, edge, or corner site modeled with $Mg_9O_9Mg^*_{17}$ (terrace), $Mg_{10}O_{10}Mg^*_{14}$ (edge), and $Mg_4O_4Mg^*_6$ (corner) PC-embedded clusters, Table 2. In all cases the interaction is very weak and originates entirely from polarization contributions. After BSSE correction the binding energies are always smaller than 0.2 eV, indicating that the alkali metal could be stabilized at one of these sites only at very low temperatures (well below liquid nitrogen). The structures obtained by geometry optimization correspond to local minima on the potential energy surface. As we will see below, adsorption at the oxygen anion sites is definitely preferred, and in a few cases the alkali atom moves spontaneously from a cation to the adjacent oxygen site.

Given the weak bonding, it is not surprising that alkali atoms interacting with the surface cations are only slightly perturbed: the spin is mostly localized on Na and the a_{iso} values are very close to those of the free atom; the corresponding values for the ^{25}Mg are negligible, Table 2. The small reduction of a_{iso}(Na) indicates a mixing of the 3s with the 3p orbitals induced by the surface electric field. The same effect can be obtained by placing the Na atom in a uniform electric field $F = 0.01$ au. A field of this magnitude induces a polarization of the valence electron of Na, which leads to a_{iso}(Na) = 288.0 G, somewhat smaller than that computed for the atom adsorbed on the cation sites, Table 2. We conclude that the surface cations do not play a role in the adsorption of alkali-metal atoms on MgO.

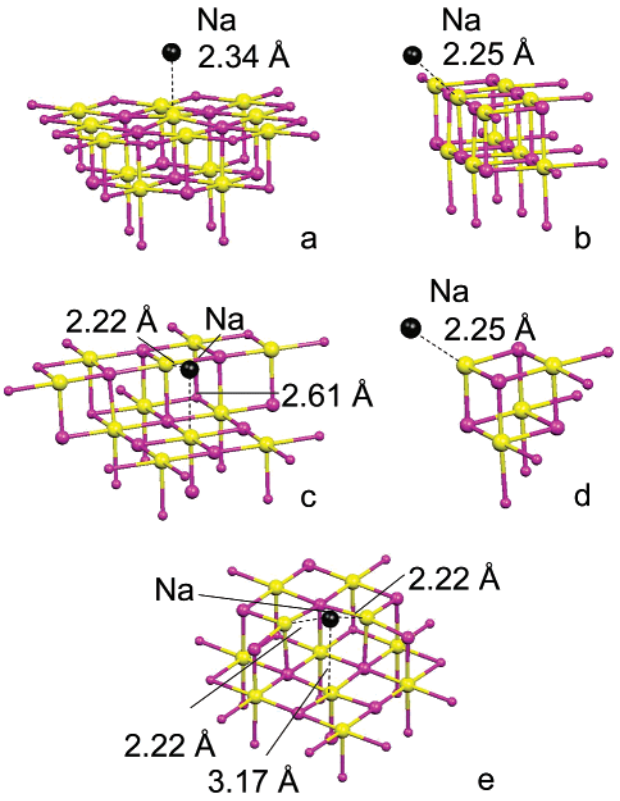

Figure 1. PC-embedded models of a Na atom adsorbed on oxide anions at various sites of the MgO surface. (a) $O_{13}Mg_9Mg^*_{20}$ terrace; (b) $O_{10}Mg_{10}Mg^*_{14}$ edge; (c) $O_{11}Mg_{10}Mg^*_{18}$ step; (d) $O_4Mg_4Mg^*_6$ corner; (e) $O_{11}Mg_{11}Mg^*_{18}$ anionic reverse corner. Large dark spheres, Mg; white spheres, O; small dark spheres, Mg*.

3.1.2. Interaction of Alkali-Metal Atoms with O^{2-} Anions. Here we consider the adsorption of Na on O^{2-} anions located at terrace, edge, step, corner, and anionic reverse corner. The sites have been modeled with the following PC-embedded clusters: $O_{13}Mg_9Mg^*_{20}$ (terrace), $O_{10}Mg_{10}Mg^*_{14}$ (edge), $O_{11}Mg_{10}$-Mg^*_{18} (step), $O_4Mg_4Mg^*_6$ (corner), and $O_{11}Mg_{11}Mg^*_{18}$ (anionic reverse corner), Figure 1a−e and Table 3. A Na atom forms relatively strong bonds with the O anions of the surface. D_e goes from 0.39 eV on a terrace, Figure 1a, to 1.56 eV on the reverse corner, Figure 1e, where Na interacts with three O anions. There is an almost linear increase of the binding energy by reducing the coordination of the O anion: going from the terrace, to the edge, and to the corner, D_e goes from 0.39, to 0.66, to 1.05 eV, respectively, Table 3. On a step, Figure 1c, characterized by the presence of a O_{4c} and an O_{5c} ion, Na is bound only to the O_{4c} site with a D_e of 0.76 eV.

The ionization potential (IP) of the adsorbed Na atom decreases considerably, going from 5.4 eV in the gas-phase to about 2−3 eV on the surface, with a minimum IP for the anionic reverse corner, 2.3 eV, and a maximum for the edge, 3.5 eV, Table 3. Thus, once the alkali metal is deposited on the surface, its ionization becomes considerably easier.

The results have been extended to Li and K, but we restrict the analysis to the corner O_{3c} anion. The binding energy decreases along the series Li, Na, K, while the nature of the bonding is very similar, with the electron largely localized on

TABLE 3: Adsorption Properties of a Neutral Na Atom on Various Anion Sites of the MgO Surface as Modeled by PC-Embedded Clusters[a]

	terrace	edge	step	corner	MgO_{ARC}
d(Na−O), Å	2.34	2.25	2.22	2.25	2.22
D_e, eV	0.64	0.75	0.93	1.13	1.72
D_e (BSSE), eV	0.39	0.66	0.76	1.05	1.56
q(Na)	0.16	0.20	−0.08	0.08	0.12
spin(Na)	1.07	0.73	1.09	0.90	0.83
IP,[b] eV	3.06	3.48	2.62	2.88	2.33
a_{iso} (Na), G	204.4	195.2	155.1	147.9	82.2
B_1, G	−1.2	−1.1	−1.4	−1.3	−2.2
B_2, G	−1.2	−1.1	−1.4	−1.3	−2.1
B_3, G	+2.4	+2.2	+2.8	+2.6	+4.4

[a] d(Na−Mg) = shortest Na−Mg distance; D_e = dissociation energy; D_e(BSSE) = dissociation energy corrected by the BSSE; ω_e = Na−MgO vibrational frequency; q(Na) = net charge on Na from Mulliken population; spin(Na) = spin population on Na; IP = ionization potential; a_{iso} = isotropic hyperfine coupling constant; B_n = anisotropic hyperfine coupling constant. [b] Adiabatic ionization potential MgO/Na → MgO/$Na^+ + e^-$.

TABLE 4: Adsorption Properties of a Li and K Atoms and Li^+ and K^+ Cations on a Corner O^{2-} Site of the MgO Surface as Modeled by PC-Embedded Clusters[a]

	Li	Li^+	K	K^+
d(M−O), Å	1.72	1.70	2.46	2.42
D_e, eV	1.97	4.75	0.99	2.97
q(M)	0.01	0.77	0.03	0.94
IP, eV	2.83		2.51	
spin(M)	0.84		0.93	
a_{iso}(M), G	50.6		42.1	

[a] d(M−O) = shortest M−O distance; D_e = dissociation energy; q(M) = net charge on M from Mulliken population; IP = ionization potential; spin(M) = spin population on M; a_{iso} = isotropic hyperfine coupling constant.

the alkali atom, Table 4. Li is bound by almost 2 eV, while K is bound by 1 eV. In both cases the IP of the adsorbed alkali is below 3 eV.

Differently from the adsorption on cations, here polarization effects are not the only bonding mechanism. It is difficult to imagine the occurrence of large charge transfer between Na and the O^{2-} ion; the O anions of MgO are in fact almost fully reduced, with a net charge close to −2. On the other hand, the Na atom has a small electron affinity, EA = 0.59 eV (experimental EA = 0.55 eV), and some charge transfer from the O to the alkali metal is possible, at least in principle. However, both the analysis of the wave function and the Mulliken charges indicate that the bonding has a more covalent nature, with typical hybridization of metal and oxide states at the interface. The unpaired electron remains largely localized on Na, Table 3, but the composition of the wave function changes dramatically, with strong transfer of the spin density from the s to the p orbitals. On a O_{3c} anion, a_{iso} for Li, Na, and K is 51, 148, and 42 G, respectively, Tables 3 and 4, while the corresponding gas-phase values are 155 G (Li), 335 G (Na), and 84 G (K), Table 1. The reduction of a_{iso} by more than a factor 2 does not imply the occurrence of a charge transfer to the surface. In fact, in all cases the charge on the alkali is close to zero and the spin population is close to one. On the anionic reverse corner, MgO_{ARC}, Figure 1e, a_{iso}(Na) is very low, 82 G, Table 3, despite the absence of charge transfer from Na to the surface. The importance of this result for the interpretation of the experimental EPR spectra will be discussed in the following (see section 3.3).

The results reported above have been obtained with PC-embedded clusters. Of course, the occurrence of a charge transfer could be influenced by the inclusion of long-range polarization effects. To check this point the calculations have been repeated with SM-embedded clusters for two sites, the terrace and the step, see Table 5. The QM part is $O_{14}Mg_9Mg^*_{21}$ for the terrace and $O_{13}Mg_{13}Mg^*_{17}$ for the step (for other details about the size of regions I and II see Table 5). The properties of Na adsorbed on a terrace obtained with the SM-embedded cluster, Table 5, are very close to those derived from PC-embedded clusters, Table 3. The major deviation is in the binding energy (0.64 eV versus 0.48 eV computed without BSSE) but the slightly larger value obtained with PC-embedded clusters is most likely due to the larger O basis set (see section 2). The other quantities, geometry, spin distribution, and a_{iso}, are quite similar. Some differences in the electron distribution are found in the adsorption at step. In the SM-embedding the unpaired electron is more delocalized over the entire site as shown for instance by the smaller value of a_{iso}(Na). This can be quite relevant for irregular surface sites where particular features of the electrostatic potential may result in the partial or complete dissociation of the electron from the adsorbed Na atom. For this reason, adsorption sites which may lead to a strong polarization or a complete transfer of the valence electron of Na have been investigated with SM-embedded clusters (see section 3.3).

TABLE 5: Adsorption Properties of a Na Atom and of a Na^+ Cation on O^{2-} Terrace and Step Sites of the MgO Surface as Modeled by SM-Embedded Clusters[a]

	Na		Na^+	
	terrace	step	terrace	step
d(Na−O), Å	2.37	2.23	2.11	2.16
D_e, eV	0.48	0.99	3.75	4.03
q(Na)	0.27	−0.09	0.72	0.39
IP, eV	2.15	2.38		
spin(Na)	1.07	0.57		
a_{iso}(Na), G	216	138		

[a] Terrace: $Mg_9O_{14}Mg^*_{21}$; region I is represented by 856 classical shell model ions; region II consists of 2300 point charges. Step: $Mg_{13}O_{13}Mg^*_{17}$; region I is represented by 752 classical shell model ions; region II consists of 2205 point charges. d(Na−Mg) = shortest Na−Mg distance; D_e = dissociation energy; q(Na) = net charge on Na from Mulliken population; IP = ionization potential; spin(Na) = spin population on Na; a_{iso} = isotropic hyperfine coupling constant.

TABLE 6: Adsorption Properties of a Na^+ Cation on Various Anion Sites of the MgO Surface as Modeled by PC-Embedded Clusters[a]

	terrace	edge	step	corner	MgO_{ARC}
d(Na−O), Å	2.15	2.14	2.16	2.09	2.13
D_e, eV	3.00	2.68	3.73	3.67	4.80
q(Na)	1.23	0.90	0.87	0.93	0.81

[a] d(Na−O) = shortest Na−O distance; D_e = dissociation energy; q(Na) = net charge on Na from Mulliken population.

3.2. Adsorption of Alkali Metal Cations. The creation of paramagnetic centers by doping the surface with alkali-metal atoms implies that the valence electron of the alkali metal is trapped to a preexisting diamagnetic site with formation of an alkali-metal cation. The cations formed in this way can be stabilized at surface anions, partly compensating for the cost of the ionization. The binding energy of Li^+, Na^+, or K^+ to the MgO surface sites is therefore of interest for the study of the ionization mechanism. A Na^+ ion has been adsorbed on various O^{2-} sites of the MgO surface, Table 6. The binding energies go from 3.0 eV on the terrace to 4.8 eV on a anionic reverse corner. The interaction is very strong also with a corner or a step site, 3.7 eV. In some cases (MgO_{ARC} or step), the Na^+ ion occupies a position which corresponds almost exactly to that

which would be occupied by a Mg^{2+} ion by extending the lattice. The Na^+-O^{2-} distances are slightly shorter than for the neutral complexes and the net charge on sodium remains close to +1, Table 6.

Of course, the adsorption energies of a Na^+ ion on MgO calculated with PC-embedded clusters suffer from the limitation that long-range polarization is not included. The calculations have been repeated for two sites, the terrace and the step, using the SM-embedded clusters, Table 5. The distances are close to those obtained with the PC-embedded cluster, while the adsorption energies are larger. The effect of the lattice polarization is more pronounced for adsorption on a terrace than adsorption on a step: the energy difference between PC- and SM-embedded clusters is of 0.75 and 0.30 eV, respectively (in this comparison one should take into account that a different basis set has been used for the oxide anions of the SM-embedded cluster, see section 2; for the same reason, the results of the Mulliken charges are somewhat different in the two cases).

Strong adsorption energies, correlated to the metal−oxide distance hence to the size of the cation, are found also for the other alkali-metal cations, Tables 4 and 6: the binding of Li^+, Na^+, and K^+ on a O_{3c} anion is 4.75, 3.67, and 2.97 eV, respectively, while the $O_{3c}-M^+$ distance increases along the series, 1.72 Å (Li), 2.09 Å (Na), and 2.42 Å (K), Tables 4 and 6.

3.3. Ionization of Alkali Metal Atoms on MgO. In the previous sections we have seen that alkali-metal atoms bind at oxide anions with bond strengths of the order of 1 eV or more and that the unpaired electron remains mostly localized on the alkali metal. The cost to remove the valence electron of adsorbed Na is ≈2−3 eV only, compared to the 5.4 eV needed to ionize the free atom. This means that surface sites which can trap an electron with EA's of 2−3 eV may cause the ionization of the alkali atom and lead to the formation of paramagnetic defect centers on the surface.

The existence of this reaction path is actually experimentally proven by the EPR spectra observed in the very early stages of the deposition (small doses of the metal evaporated onto the solid).[70−73] The spectra recorded by contacting high surface area polycrystalline MgO with atomic hydrogen and alkali metals (Li, Na, K, Rb), adapted from ref 71, are reported in Figure 2a−e. In all cases the sample turns pale blue after the interaction revealing that color centers are formed. This is confirmed by the observed EPR spectra (Figure 2), which exhibit an axial signal, centered at *g* values slightly lower than the free spin value, typical of surface-trapped electrons. Although all the alkali metals employed have nonzero nuclear spin (3/2 for Li, Na, K, 5/2 and 3/2 for ^{85}Rb and ^{87}Rb, respectively) and rather different nuclear magnetic moments, all the spectra look very similar. In particular no detectable electron−nucleus hyperfine interaction is observed. This indicates that the trapped electron monitored by EPR has no (or very weak) residual interaction with the parent atom. In other words, the incoming alkali-metal atom is fully ionized. This is different from the spectrum generated by reaction of the MgO matrix with H atoms (Figure 2a), which is characterized by a doublet of 2.07 G splitting, which is the fingerprint of the well-known F_s^+(H) centers (a trapped electron in interaction with a nearby OH group). The spectra in Figure 2 indicate that at the surface of fully dehydrated MgO there are sites capable of inducing a process of ionization of alkali-metal atoms. In this section we consider possible candidates for this process.

Recently, considerable attention has been given to the MgO surface sites which can transform into electron traps by chemical

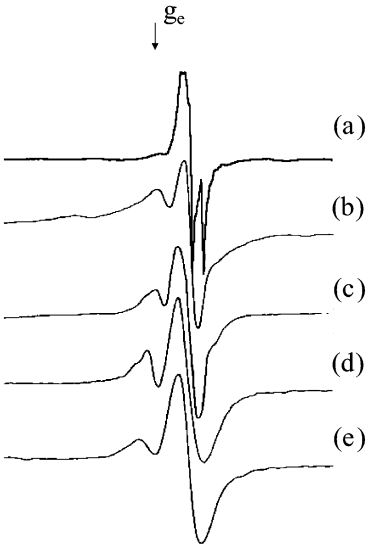

Figure 2. EPR spectra of F_s^+ centers on MgO after exposure to (a) H atoms, (b) Li, (c) Na, (d) K, and (e) Rb vapors. All the spectra are recorded at room temperature at a modulation frequency of 100 kHz with 1 G modulation amplitude and 1 mW microwave power. Spectra b−e for Li, Na, K, and Rb are adapted from ref 71; Spectrum a is unpublished. Further experimental details about deposition method and spectral resolution can be found in ref 71.

treatment of the sample.[74−76] On MgO, molecular hydrogen dissociates into H^+ and H^- species which under UV irradiation form new EPR-active centers consisting of one electron trapped near a proton, $MgO(H^+)(e^-)_{trapped}$.[27,56] Another way to produce trapped electrons at the MgO surface is by depositing a low dosage of alkali metals. In this case a possible surface trap is of course the bare oxygen vacancy, F_S^{2+}:[70−72]

$$F_S^{2+} + M^{\bullet}(g) \rightarrow F_S^{\bullet +} + M^+_{ads} \qquad (3)$$

The presence of F_S^{2+} diamagnetic centers is very difficult to verify experimentally. Moreover, the high formation energy of F_S^{2+} defects suggests that their number at thermal equilibrium should be relatively small. This has stimulated several authors to look for other potential electron trapping sites at the MgO surface.[41,76] For instance, a double Mg and O vacancy, V_{MgO},[76] is a neutral defect much easier to form than F_S^{2+}, which can trap one electron.[74,75] Also low-coordinated Mg^{2+} ions, located at kinks and corners, can serve as electron traps.[76,52] However, all these centers are "shallow traps", where the electron is bound by 1−1.5 eV only. These energies are large enough that the traps are stable up to room temperature but cannot explain the color change which accompanies the creation of the paramagnetic centers.[41]

Let us consider reaction 3. Here the key parameter is the EA of the F_S^{2+} center. To model a F_S^{2+} center we used two SM-embedded clusters. Cluster A, symmetrically centered around the vacancy, consists of a $O_{13}Mg_9Mg^*_{21}$ QM part with region I and region II containing 856 polarizable ions and 2300 PC's, respectively; cluster B contains a larger number of QM atoms, $O_{16}Mg_{17}Mg^*_{21}$, to allow for the adsorbance of a Na atom in the vicinity of the vacancy, Figure 3; region I and region II contain 845 polarizable ions and 2300 PC's, respectively. The adiabatic EA for F_S^{2+} is 3.47 eV with cluster A and 4.14 eV with cluster B. Since the IP of an adsorbed Na atom on a terrace site is about 2 eV, Table 5, it follows that it is energetically favorable to dissociate Na in the presence of F_S^{2+} centers with a net energy gain of 1.5−2 eV. This number is computed for isolated, noninteracting fragments, i.e., the F_S^+ center and an

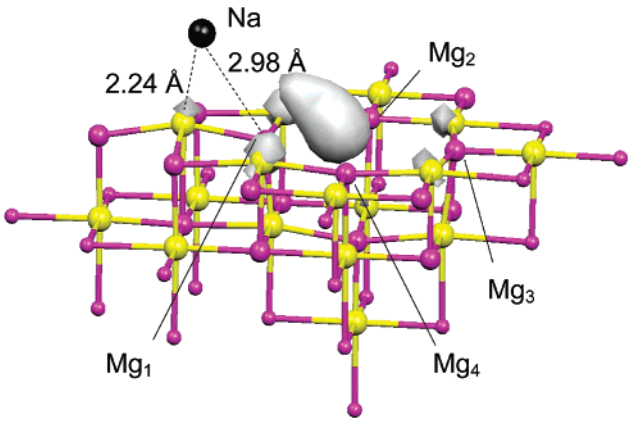

Figure 3. SM-embedded cluster used to model a Na atom adsorbed near an oxygen vacancy, F_S^{2+}. The figure shows also an iso-contour surface of the spin density. The structure corresponds to the $O_{16}Mg_{17}$-Mg^*_{21} quantum-mechanical (QM) part in our SM-embedded clusters. Region I is represented by 845 classical shell model ions. The cluster is then surrounded by 2300 point charges (region II). Only the QM ions are shown for simplicity. Large dark spheres, Mg; white spheres, O; small dark spheres, Mg*.

TABLE 7: Adsorption Properties of a Na Atom Adsorbed near a Bare Oxygen Vacancy (F_S^{2+}) and a Cationic Reverse Corner (MgO_{CRC}) as Modeled by SM and PC-Embedded Clusters[a]

initial	$Na(g) + F_S^{2+}$		$Na(g) + MgO_{CRC}$	
final	$Na^+_{ads} - F_S^+$		$MgO_{CRC}(Na^+)(e^-)_{trapped}$	
	SM-embedding	PC-embedding	SM-embedding	PC-embedding
d(Na−O), Å	2.24	2.36	2.24	2.34
D_e, eV	0.49	0.70	1.00	0.89
q(Na)	0.61	0.65	0.06	0.27
IP, eV	5.77	9.63	3.06	4.22
$IP_{vertical}$, eV	6.33	10.43	3.66	4.68
T_e (TD-DFT), eV		1.18	1.28	1.37
		2.83	1.94	2.26
		2.98	2.19	2.31
spin(Na)	0.61	0.10	0.25	0.18
a_{iso}(Na), G	98.2	30.7	109.8	138.9
B_1, G		−0.4		−2.1
B_2, G		−0.3		−1.8
B_3, G		+0.7		+3.9
$a_{iso}(Mg_1)$, G	−8.3	−9.2	−10.5	−8.9
$a_{iso}(Mg_{2,3,...})$, G	−1/−2	−1/−3	−2/−3	0/−4

[a] d(Na−O) = shortest Na−O distance; D_e = dissociation energy; IP = ionization potential; $IP_{vertical}$ = vertical ionization potential; T_e(TD-DFT) = transition energy computed at the TD-DFT level; spin(Na) = spin population on Na; a_{iso} = isotropic hyperfine coupling constant; B_n = anisotropic hyperfine coupling constant.

adsorbed Na^+ ion separated by infinite distance. If the distance is decreased, however, the two centers will give rise to a Coulomb repulsion which increases with the inverse of the distance. At very short distances the Coulomb repulsion between F_S^+ and Na^+ can prevail so that no ionization occurs.

To check this hypothesis we have considered a second model of F_S^{2+}, cluster B, Figure 3, where a Na^+ ion has been adsorbed on a O_{5c}^{2-} anion near the vacancy. This can result into two structures, $Na^{\bullet}_{ads}$–F_S^{2+} (no charge transfer) or Na^+_{ads}–$F_S^{+\bullet}$ (charge transfer). The geometry optimization leads to a surface complex where the Na atom is 2.24 Å from the O_{5c}^{2-} ion, a distance which is between that of Na−O and Na^+−O bonds, see Table 7. The spin and charge distributions, however, clearly show the formation of a Na^+_{ads}–$F_S^{+\bullet}$ center, with the electron localized in the vacancy but polarized toward sodium, Figure 3. This system is 0.49 eV lower in energy than F_S^{2+} + Na(g),

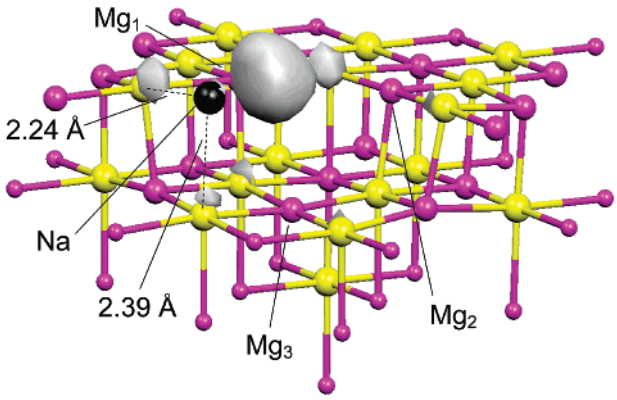

Figure 4. SM-embedded cluster used to model a Na atom adsorbed near a cationic reverse corner, MgO_{CRC}. The figure shows also an iso-contour surface of the spin density. The structure corresponds to the $O_{17}Mg_{17}Mg^*_{22}$ quantum-mechanical (QM) part in our SM-embedded clusters. Region I is represented by 795 classical shell model ions. The cluster is then surrounded by 2259 point charges (region II). Only the QM ions are shown for simplicity. Large dark spheres, Mg; white spheres, O; small dark spheres, Mg*.

Table 7. Considering that a Na atom adsorbed on a regular terrace is bound by 0.48 eV, Table 5 (SM-embedding), the process is almost thermoneutral. Thus, even for short Na^+_{ads}–$F_S^{+\bullet}$ distances the dissociation of the Na atom seems possible. Of course, as the distance of the alkali cation from $F_S^{+\bullet}$ increases, the system gains stability. This could explain the absence of hyperfine interaction with the alkali nucleus observed in the experiment for a low dosage of Na.

The conclusions are qualitatively similar using PC-embedded clusters. In fact, the EA of the F_S^{2+} center computed with the $O_{12}Mg_5Mg^*_{24}$ PC-embedded cluster is 6.65 eV, i.e., more than 2 eV larger than with the SM-embedded cluster (in the SM-embedded cluster the large lattice polarization stabilizes the F_S^{2+} center thus reducing its affinity for electrons). Therefore, with respect to an adsorbed Na atom on a terrace, the formation of noninteracting Na^+ and $F_S^{+\bullet}$ units is energetically favored by 4.41 eV (the EA of F_S^{2+}, 6.65 eV, minus the IP of Na/O_{5c}, 2.24 eV, computed with PC-embedded clusters). When the Na atom is placed in the proximity of the F_S^{2+} center, the resulting complex shows very similar characteristics to those obtained with the SM-embedded cluster, Table 7: the Na^+_{ads}–$F_S^{+\bullet}$ system is bound by 0.70 eV with respect to F_S^{2+} and a neutral Na atom, and the electron is almost entirely transferred to the cavity.

These results show unambiguously that F_S^{2+} centers, when present, can ionize alkali-metal atoms, explaining the formation of paramagnetic color centers on the surface. In this context it is worth noting that oxygen vacancies are easier to form on steps, edges, and corners.[31,37,40] Low-coordinated F^{2+} centers have not been considered here but are expected to behave in the same way. Bare F_S^{2+} centers are the *only* sites that we have identified which can give rise to reaction 1. In fact, because of the relatively high IP of adsorbed Na atoms, 2−3 eV, shallow traps such as a divacancy, a Mg_{3c}^{2+} ion, a cationic reverse corner, etc., with EA's of about 1 eV, cannot ionize the alkali metal. However, they can induce a strong polarization of the electron cloud and even result in the formation of cation−electron pairs, $(M^+)(e^-)$, as recently found for hydrogen.[56]

To check this possibility, we have considered a Na atom adsorbed in the vicinity of the cationic reverse corner, MgO_{CRC}, Figure 4 and Table 7, modeled by a SM-embedded cluster. The QM part of the cluster is $Mg_{17}O_{17}Mg^*_{22}$; region I consists of 795 polarizable ions, and region II of 2259 PC's. The same cluster has been used in the study of H_2 interaction.[56] The Na

atom was placed in a position intermediate between a O_{4c}^{2-} and a O_{5c}^{2-} anion, and the geometry optimized. In this way one forms a sort of artificial cavity defined by one of the MgO steps and by the Na atom, Figure 4. In this site Na is adsorbed with a $D_e = 1.0$ eV, Table 7, very similar to that found for a step site. The analysis of the spin density, however, clearly shows that the unpaired electron is strongly polarized toward the reverse corner, Figure 4, to such an extent that the surface complex can be described as a $(Na^+)(e^-)_{trapped}$ pair very similar to that found on the same site for hydrogen, $(H^+)(e^-)_{trapped}$.[56] This result is obtained also with a $O_{10}Mg_8Mg^*_{16}$ PC-embedded cluster, Table 7.

The electrostatic potential generated by the Na^+ ion adsorbed near a cationic reverse corner creates a deep potential for the trapped electron. The vertical IP of this center is in fact 3.7 eV, and the $(Na^+)(e^-)_{trapped}$ surface complex can give rise to electronic transitions in the visible region. To check this we have determined the excitation energies of the $MgO_{CRC}(Na^+)(e^-)_{trapped}$ center using the time-dependent density functional approach (TD-DFT). We found a first transition at 1.3 eV and two other transitions at 1.9 and 2.2 eV, Table 7, with oscillator strengths $f = 0.17$, 0.13, and 0.07, respectively, typical of strong absorptions. Electronic transitions of about 2 eV are fully consistent with experimental measurements on doped polycrystalline MgO samples, which show optical transitions due to surface color centers at 2−2.5 eV.[41]

For the case of H adsorption,[56] it has been found that also on a step site one can form a $MgO_{step}(H^+)(e^-)$ pair, in close similarity to $MgO_{CRC}(H^+)(e^-)$. Things are different when we consider a Na atom in the same position. In fact, when Na is adsorbed on a step site, the electron remains localized on Na (see also section 3.1.2). The distortion of the Na 3s electron cloud results in major changes in the hyperfine coupling constants, as will be discussed below. However, there is no formation of a $(Na^+)(e^-)_{trapped}$ pair. The reason for the different behavior of H and Na is that the proton generates a much deeper potential on the neighboring Mg sites than a Na^+ cation.

4. Discussion: Spin Distribution and Hyperfine Interactions

Experimentally, three different situations have been observed by dosing alkali metals on polycrystalline MgO, depending on the amount of metal deposited.[71]

(1) At very low coverage only the signal typical of paramagnetic centers, $g_\perp = 2.0012$, $g_{||} = 2.004$, conventionally identified with $F_S^{+\bullet}$ centers, has been observed. No coupling is seen with the Na nucleus.

(2) At higher coverage the $g_{||}$ and $g_\perp$ values become 2.0017 and 2.0010, respectively, and an hyperfine coupling with the Na nucleus is measured, $A_{||} = 68$ G and $A_\perp = 63$ G, with an a_{iso}(Na) of 64.7 G.

(3) At even higher coverages the formation of $Na_3^{\delta+}$ clusters is assumed from the measured *g*-values and hyperfine couplings.

Based on the calculations described above, one can attempt to formulate some hypothesis about the mechanism of interaction of alkali metals with MgO. At low coverage the experiments show that the trapped electron is completely separated from the Na nucleus. According to our models, this would be consistent with the classical picture of Na atoms being ionized by bare oxygen vacancies, the F_S^{2+} centers; see reaction 3. The calculations show in fact that it is energetically favorable to ionize Na and to move the resulting Na^+ ion far away from the paramagnetic $F_S^{+\bullet}$ center. In this case only the hyperfine coupling with ^{25}Mg should be observed. The calculations performed with the SM-embedded clusters for an isolated $F_S^{+\bullet}$ center give $a_{iso} = -5.3$ G for the four Mg ions in the top layer and $a_{iso} = -2.4$ G for the apical Mg atom in the second layer. The PC-embedded cluster gives similar values (−4.6 and −2.9 G, respectively). These values are almost identical to those reported by Ferrari and Pacchioni based on Hartree−Fock calculations.[35]

Another possibility is that the Na valence electron is transferred to a morphological defect which acts as a shallow trap. However, we have seen above that the energy gained by trapping the electron is not sufficient to compensate the cost of the ionization. Furthermore, the shallow traps do not explain the color of the sample following the doping with alkali metals. Thus, the most likely hypothesis is that in the initial phases of the deposition $F_S^{+\bullet}$ centers are created starting from F_S^{2+} diamagnetic precursors, i.e., according to the classical Tench proposal.[26,27] The question which remains open is the number of these sites on the surface.

Once all the F_S^{2+} sites have been saturated, the deposition of additional alkali metal atoms must involve other sites. Here various hypotheses can be formulated. The first one is that $(Na^+)(e^-)_{trapped}$ pairs form in correspondence to some specific morphological sites, like, for instance, a cationic reverse corner, a site which is representative of a whole family of electron traps on the surface. On this site, the transfer of the Na 3s electron to the cavity formed by the adsorbed atom, Figure 4, results in a strong lowering of a_{iso}(Na), which becomes 109.8 G, Table 7. This is much larger than the measured $a_{iso} = 64.7$ G but suggests that $(Na^+)(e^-)_{trapped}$ complexes may have properties close to the observed ones. The $(Na^+)(e^-)_{trapped}$ pairs are also consistent with the coloring of the sample and with the high thermal stability of the centers.

The appearance of a low isotropic hyperfine coupling constant with the alkali metal does not necessarily imply a partial ionization of the alkali metal. In fact, the calculations show that in general the bonding of a neutral alkali atom on an oxygen site results in a strong lowering of a_{iso}, see Tables 3 and 4. For some sites the effect is quite dramatic. A Na atom adsorbed on an anionic reverse corner, Figure 1e, exhibits a spin population of 0.83 and a net charge of 0.12, Table 3, indicating that virtually no charge transfer has occurred; still, a_{iso}(Na) is 82.2 G, i.e., not too far from the value measured experimentally, 64.7 G. If the analysis is extended to the dipolar part of the interaction, a surprising but probably fortuitous similarity of the computed and measured values is found (experimental tensor, $B_1 = B_2 = -1.7$ G, $B_3 = +3.4$ G; computed tensor, $B_1 = B_2 = -2.2$ G, $B_3 = +4.4$ G). However, this site has optical transitions at 0.41 ($f = 0.07$), 0.53 ($f = 0.02$), and 1.02 eV ($f = 0.08$) which cannot explain the color properties of the paramagnetic surface centers. While this seems to rule out the site of Figure 1e as a possible candidate for the observed paramagnetic centers, one can certainly conclude that there is a family of sites where the Na atoms can be stabilized, giving rise to a strong anisotropy in the spin distribution even in absence of a real dissociation of the valence electron.

Alkali-metal atoms trapped in rare gas or hydrocarbon matrixes exhibit deviations of the hyperfine interactions from the gas-phase values which have been discussed in terms of attractive and repulsive forces.[77] van der Waals attractive forces between the metal atom and the matrix cause an expansion of the atomic charge cloud leading to a decrease of the hyperfine interaction. Repulsive forces arise when the charge clouds of the atom and of the matrix overlap with a resulting increase in the hyperfine interaction.

A quantitative measure of the perturbation of the atom *n*s wave function due to the environment can be obtained from the following equation:

$$\Delta A = \frac{[a_{iso} - a(\text{free atom})]}{a(\text{free atom})} \times 100 \qquad (4)$$

ΔA values for alkali metals trapped in adamantane range from -5.6 for Li to $+4.1$ for Cs.[78] In the case of Na on MgO, the calculated ΔA values for Na on cationic sites are about -9.8, whereas the calculated values for Na adsorbed on various anion sites range from -38.9 to -75.4. When Na sits near a F_S^{2+} center and a cationic reverse corner, ΔA ranges from -70.6 and -90.8 in the first case (F_S^{2+}) and -67.2 to -58.8 in the second one. The experimental value, obtained using the values recorded in the case of the mono-alkaline center for both a_{iso} and a(free atom), is -79.5.

It has been suggested that group I metal atoms can acquire permanent dipole moments even in a total-symmetric environment as a consequence of an electronic phase transition known as a dipolar excitonic insulator transition.[79] This transition is driven primarily by changes in the host matrix density. The dipolar atomic state results from the hybridization of the normal ground state (^{2}S) with the first excited (^{2}P) state to form a new sp-hybridized atomic ground state with nonzero dipole moment. This would of course introduce hyperfine and/or *g* anisotropy in the spin Hamiltonian. It is possible that a similar hybridization can be stabilized also by the ionic MgO matrix.

5. Conclusions

We have studied with DFT cluster calculations the bonding of alkali-metal atoms deposited on MgO. The alkali atoms always prefer to bind at the surface oxide anions, with binding energies which range from 0.4 to 1.6 eV, depending on the adsorption site. On these sites the valence electron remains largely localized on the alkali atom, with little charge transfer to the surface. The appearance of the typical signal of paramagnetic electron centers on the MgO surface implies that the alkali atom donates its valence electron to a preexisting trapping site. At very low coverage, the best candidate for this process is the bare oxygen vacancy, F_S^{2+}, which by addition of one electron transforms into the EPR active $F_S^{+\bullet}$ center. The resulting M^+ cation cannot remain in the vicinity of the F_S^+ center because of the repulsive interaction of the two charged entities, thus explaining the absence of hyperfine interaction of the trapped electron with the alkali metal. Other potential sites for electron trapping, like cations at the corners, divacancies, reverse corners, etc., have electron affinities which are not sufficient to compensate for the relatively high ionization potential of the adsorbed alkali atoms.

Morphological defects, however, play an important role as the amount of deposited alkali metal is increased. In fact, on some of these sites, e.g., on a cationic reverse corner, the formation of $(M^+)(e^-)_{trapped}$ pairs could account for the EPR signal of the trapped electron, its hyperfine interaction with a nearby alkali metal, and the color of the sample. The presence of the adsorbed alkali-metal cation near one of the sites provides a deep potential for the electron which can explain the observed properties of the alkali-doped MgO surface. Similar sites have been recently found to be responsible for the complex reaction of molecular hydrogen with MgO and for the subsequent formation of $(H^+)(e^-)_{trapped}$ centers under the effect of UV irradiation.[56] Therefore, the cationic reverse corner and similar morphological sites form a new class of defects at the surface of MgO which can explain the formation of paramagnetic color centers under various chemical treatments.

Acknowledgment. This work has been supported by the "Italian INFM" through the PRA project ISADORA. We thank A. L. Shluger and P. V. Sushko for providing a version of the Guess code and for useful discussions.

References and Notes

(1) Freund, H.-J. *Surf. Sci.* **2002**, *500*, 271.
(2) Lambert, R. M.; Pacchioni, G., Eds. *Chemisorption and Reactivity on Supported Clusters and Thin Films*; NATO ASI Series E; Kluwer: Dordrecht, 1997; Vol. 331.
(3) (a) Onishi, H.; Egawa, C.; Aruga, T.; Iwasawa, Y. *Surf. Sci.* **1987**, *191*, 479. (b) Brause, M.; Ochs, D.; Gunster, J.; Mayer, T.; Braun, B.; Puchin, V.; Maus-Friedrichs, W.; Kempter, V. *Surf. Sci.* **1997**, *383*, 216. (c) Kendelewicz, T.; Liu, P.; Brown, G. E.; Nelson, E. J.; Pianetta, P. *Surf. Sci.* **1996**, *352*, 451. (d) Snyder, J. A.; Jaffe, J. E.; Gutowski, M.; Lin, Z.; Hess, A. C. *J. Chem. Phys.* **2000**, *112*, 3014.
(4) Pacchioni, G. In: *The Chemical Physics of Solid Surfaces−Oxide Surfaces*; Woodruff, P., Ed.; Elsevier: Amsterdam, 2000; Vol. 9, pp 94−135.
(5) Pacchioni, G. *Surf. Rev. Lett.* **2000**, *7*, 277.
(6) He, J.; Moller, P. *Chem. Phys. Lett.* **1986**, *129*, 13.
(7) Kubo, M.; Miura, R.; Yamauchi, R.; Vetrivel, R.; Miyamoto, A. *Appl. Surf. Sci.* **1995**, *89*, 131.
(8) Hu, A.; Neyman, K. M.; Staufer, M.; Belling, T.; Gates, B. C.; Rösch, N. *J. Am. Chem. Soc.* **1999**, *121*, 4522.
(9) Bogicevic, A.; Jennison, D. R. *Surf. Sci.* **1999**, *437*, L741.
(10) Sanchez, A.; Abbet, S.; Heiz, U.; Schneider, W.-H.; Häkkinen, H.; Barnett, R. N.; Landman, U. *J. Phys. Chem. A* **1999**, *103*, 9573.
(11) Zhukovskii, Y. F.; Kotomin, E. A.; Jacobs, P. W. M.; Stoneham, A. M.; Harding, J. H. *J. Phys.: Condens. Matter* **2000**, *12*, 55.
(12) Goellner, J. F.; Neyman, K. M.; Mayer, M.; Nörtermann, F.; Gates, B. C.; Rösch, N. *Langmuir* **2000**, *16*, 2736.
(13) Abbet, S.; Sanchez, A.; Heiz, U.; Schneider, W.-D.; Ferrari, A. M.; Pacchioni, G.; Rösch, N. *J. Am. Chem. Soc.* **2000**, *112*, 3453.
(14) Zhukovskii, Y. F.; Kotomin, E. A.; Jacobs, P. W. M.; Stoneham, A. M. *Phys. Rev. Lett.* **2000**, *84*, 1256.
(15) Stracke, P.; Krischok, S.; Kempter, V. *Surf. Sci.* **2001**, *473*, 86.
(16) Giordano, L.; Goniakowski, J.; Pacchioni, G. *Phys. Rev. B* **2001**, *64*, 075417.
(17) Abbet, S.; Riedo, E.; Brune, H.; Heiz, H.; Ferrari, A. M.; Giordano, L.; Pacchioni, G. *J. Am. Chem. Soc.* **2001**, *123*, 6172.
(18) Abbet, S.; Heiz, U.; Häkkinen, H.; Landman, U. *Phys. Rev. Lett.* **2001**, *86*, 5950.
(19) Kim, Y. D.; Stulz, J.; Wei, T.; Goodman, D. W. *J. Phys. Chem. B* **2002**, *106*, 6827.
(20) Bogicevic, A.; Jennison, D. R. *Surf. Sci. Lett.* **2002**, *515*, L481.
(21) Yang, Z.; Wu, R.; Zhang, Q.; Goodman, D. W. *Phys. Rev. B* **2002**, *65*, 155407.
(22) Lopez, N.; Paniagua, J. C.; Illas, F. *J. Chem. Phys.* **2002**, *117*, 9445.
(23) Moseler, M.; Häkkinen, H.; Landman, U. *Phys. Rev. Lett.* **2002**, *89*, 176103.
(24) Pacchioni, G.; Ferrari, A. M.; Giamello, E. *Chem. Phys. Lett.* **1996**, *255*, 58.
(25) Chiesa, M.; Giamello, E.; Paganini, M. C.; Pacchioni, G.; Soave, R.; Murphy, D. M.; Sojka, Z. *J. Phys. Chem. B* **2001**, *105*, 497.
(26) Tench, A. J.; Nelson, R. L. *J. Colloid Interface Sci.* **1968**, *26*, 364.
(27) Tench, A. J. *Surf. Sci.* **1971**, *25*, 625.
(28) Scorza, E.; Birkenheuer, U.; Pisani, C. *J. Chem. Phys.* **1997**, *107*, 9645.
(29) Sharma, R. R.; Stoneham, A. M. *J. Chem. Soc., Faraday Trans.* **1976**, *2*, 913.
(30) Gibson, A.; Haydock, R.; LaFemina, J. P. *Phys. Rev. B* **1994**, *50*, 2582.
(31) Kantororovich, L. N.; Holender, J. M.; Gillan, M. J. *Surf. Sci.* **1995**, *343*, 221.
(32) Castanier, E.; Noguera, C. *Surf. Sci.* **1996**, *364*, 1.
(33) Finocchi, F.; Goniakowski, J.; Noguera, C. *Phys. Rev. B* **1999**, *59*, 5178.
(34) Pisani, C.; Corà, F.; Dovesi, R.; Orlando, R. *J. Elec. Spectrosc.* **1994**, *96*, 1.
(35) Ferrari, A. M.; Pacchioni, G. *J. Phys. Chem.* **1995**, *99*, 17010.
(36) Susko, P. V.; Shluger, A. L.; Catlow, C. R. A. *Surf. Sci.* **2000**, *450*, 153.
(37) Pacchioni, G.; Pescarmona, P. *Surf. Sci.* **1998**, *412/413*, 657.
(38) Illas, F.; Pacchioni, G. *J. Chem. Phys.* **1998**, *108*, 7835.
(39) Sousa, C.; Pacchioni, G.; Illas, F. *Surf. Sci.* **1999**, *429*, 217.

(40) Giamello, E.; Paganini, M. C.; Murphy, D.; Ferrari, A. M.; Pacchioni, G. *J. Phys. Chem. B* **1997**, *101*, 971.
(41) Paganini, M. C.; Chiesa, M.; Giamello, E.; Coluccia, S.; Martra, G.; Murphy, D. M.; Pacchioni, G. *Surf. Sci.* **1999**, *421*, 246.
(42) Becke, A. D. *J. Chem. Phys.* **1993**, *98*, 5648.
(43) Lee, C.; Yang, W.; Parr, R. G. *Phys. Rev. B* **1988**, *37*, 785.
(44) Pacchioni, G.; Ferrari, A. M.; Marquez, A. M.; Illas, F. *J. Comput. Chem.* **1997**, *18*, 617.
(45) Cundari, T. R.; Stevens, W. J. *J. Chem. Phys.* **1993**, *98*, 5555.
(46) Winter, N. W.; Pitzer, R. M. *J. Chem. Phys.* **1988**, *89*, 89.
(47) Nygren, M. A.; M. Petterson, L. G.; Barandiaran, Z.; Seijo, L. *J. Chem. Phys.* **1994**, *100*, 2010.
(48) Mejias, J. A.; Marquez, A. M.; Fernandez Sanz, J.; Fernandez-Garcia, M.; Ricart, J. M.; Sousa, C.; Illas, F. *Surf. Sci.* **1995**, *327*, 59.
(49) Stevens, W. J.; Basch, H.; Krauss, M. J. *J. Chem. Phys.* **1984**, *81*, 6026.
(50) Ferrari, A. M.; Soave, R.; D'Ercole, A.; Pisani, C.; Giamello, E.; Pacchioni, G. *Surf. Sci.* **2001**, *479*, 83.
(51) Frisch, M. J. et al., *Gaussian 98*, Revision A.6; Gaussian Inc.: Pittsburgh, PA, 1998.
(52) Sushko, P. V.; Shluger, A. L.; Baetzold, R. C.; Catlow, C. R. A. *J. Phys.: Condens. Matter* **2000**, *12*, 8257.
(53) Dennis, J. E.; Sabel, R. *Numerical Methods for Unconstrained Optimization and Nonlinear Equations*; Prentice-Hall: Englewood Cliffs, NJ, 1983.
(54) Francl, M. M.; Petro, W. J.; Hehre, W. J.; Binkley, J. S.; Gordon, M. S.; De Frees, D. J.; Pople, J. A. *J. Chem. Phys.* **1982**, *77*, 3654.
(55) Hehre, W. J.; Ditchfield, R.; Pople, J. A. *J. Chem. Phys.* **1972**, *56*, 2257.
(56) Ricci, D.; Di Valentin, C.; Pacchioni, G.; Sushko, P. V.; Shluger, A. L.; Giamello, E. *J. Am. Chem. Soc.* **2003**, *125*, 738.
(57) The atomic polarizability, α, has been computed from the induced dipole moment in the presence of a uniform electric field, according to the formula $\mu = \alpha F$.
(58) *CRC Handbook of Chemistry and Physics*; CRC Press: Boca Raton, FL, 1998.
(59) Koh, A. K.; Miller, D. J. *Atomic Data and Nucl. Data Tables* **1985**, *33*, 235.
(60) Boys, S. F.; Bernardi, F. *Mol. Phys.* **1970**, *19*, 553.
(61) Casida, M. E.; Jamorki, C.; Casida, K. C.; Salahub, D. R. *J. Chem. Phys.* **1998**, *108*, 4439.
(62) Stratmann, R. E.; Scuseria, G.; Frisch, M. *J. Chem. Phys.* **1998**, *109*, 8218.
(63) Görling, A.; Heinze, H. H.; Ruzankin, S. P.; Staufer, M.; Rösch, N. *J. Chem. Phys.* **1999**, *110*, 2785.
(64) Raghavachari, K.; Ricci, D.; Pacchioni, G. *J. Chem. Phys.* **2002**, *116*, 825.
(65) Weil, J. A.; Bolton, J. R.; Wertz, J. E. *Electron Paramagnetic Resonance*; John Wiley & Sons: New York, 1994.
(66) Neyman, K. M.; Vent, S.; Pacchioni, G.; Rösch, N. *Nuov. Chim.* **1997**, *19*, 1743.
(67) Yudanov, I.; Pacchioni, G.; Neyman, K.; Rösch, N. *J. Phys. Chem. B* **1997**, *101*, 2786.
(68) Alfonso, D. R.; Jaffe, J. E.; Hess, A. C.; Gutowski, M. *Surf. Sci.* **2000**, *466*, 111.
(69) Ferrari, A. M.; Pacchioni, G. *J. Phys. Chem.* **1996**, *100*, 9032.
(70) Giamello, E.; Ferrero, A.; Coluccia, S.; Zecchina, A. *J. Phys. Chem.* **1991**, *95*, 9385.
(71) Giamello, E.; Murphy, D.; Ravera, L.; Coluccia, S.; Zecchina, A. *J. Chem. Soc., Faraday Trans.* **1994**, *90*, 3167.
(72) Murphy, D.; Giamello, E. *J. Phys. Chem.* **1995**, *99*, 15172.
(73) Chiesa, M.; Paganini, M. C.; Giamello, E.; Murphy, D. M. *J. Phys. Chem. B* **2001**, *105*, 10457.
(74) Ojamäe, L.; Pisani, C. *J. Chem. Phys.* **1998**, *109*, 10984.
(75) Ricci, D.; Pacchioni, G.; Sushko, P. V.; Shluger, A. L. *J. Chem. Phys.* **2002**, *117*, 2844.
(76) Sushko, P. V.; Gavartin, J. L.; Shluger, A. L. *J. Phys. Chem. B* **2002**, *106*, 2269.
(77) Jen, C. K.; Bowers, V. A.; Cochran, E. L.; Foner, S. N. *Phys. Rev.* **1962**, *126*, 1749.
(78) Jones, R.; Howard, J. A.; Joly, H. A.; Edwards, P. P.; Singer, R. J. *Magn. Reson. Chem.* **1995**, *33*, S98.
(79) Logan, D. E. *J. Chem. Phys.* **1987**, *86*, 234.